Deep Resources Engineering 2 (2025) 100169

Contents lists available at ScienceDirect

Deep Resources Engineering

journal homepage: www.keaipublishing.com/en/journals/deepre/

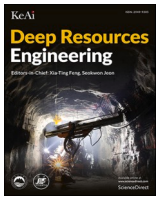

Short Communication

Thermal performance of CO_2 energy piles: A comparison with water

Linxiao Zhou [a], Haobin Liang [a,b], Deheng Wei [a], Yixiang Gan [a,*]

[a] School of Civil Engineering, The University of Sydney, Australia
[b] Building Environment and Energy Engineering, The Hong Kong Polytechnic University, Hong Kong

ARTICLE INFO

Keywords:
Geothermal energy pile (GEP)
Supercritical carbon dioxide (sCO_2)
Ragone plot

ABSTRACT

Geothermal energy piles (GEPs) buried into the deep underground are typically integrated with the circulating pipe inside the piles, where the most common heat transfer fluid (HTF) is water. Liquified carbon dioxide (CO_2), as an alternative HTF to water, is more energy-saving by its density difference and circulation in exothermic and endothermic processes, and has a more extensive application for its usability below zero degrees Celsius. In this study, thermal performances of CO_2 and H_2O in 10-h-long daily operation time in the GEP system are modelled using a finite element method (FEM). Isolated influences of temperatures and pressures on HTF performances in a small-scale single-layer tube embedded in field-scale soils are investigated. The Ragone plot, with the Péclet number of HIF being the key indicator, is introduced to evaluate such performances. The results quantitatively show that CO_2 and water in GEPs have a comparable heat extraction rate; although GEPs circulated with CO_2 consume a lower average power, a higher accumulatively extracted energy than water is encountered when operated under a similar Péclet number. It is also found that, to acquire the same system power efficiency, CO_2-GEP could respectively reach up to 4 times the power efficiency and 10 times the energy density than those of water.

1. Introduction

With high global energy prices and new environmental policies, the reliance on non-sustainable resources needs to be reduced. Strategies, such as lowering the use of fossil fuels and reducing greenhouse gas emissions [1-4], should be implemented into the renewable systems to achieve carbon neutrality target [5,6]. One of such systems increased considerably over the past twenty years is known as the geothermal energy pile (GEP) system. Consequently, a substantial amount of research has been dedicated to the thermal performance of such foundations subjected to their interactions with surrounded soils.

Geothermal loads can be idealised as imposed heat sources. Basically, the underground temperature is nearly transverse-constant at the shallow depth, in a range of 5–30 degree Celsius (°C) depending on the location [7,8]. The constant underground temperature allows cooling and heating underground constructions in summer and winter, respectively by the spontaneous heat exchange [9-12]. The utilisation of geothermal energy starts from the geothermal ground heat exchangers (GHEs), and evolves into the vertically aligned GEPs as an alternative system [13,14]. Within GEPs, soils function as the energy extraction and storage media.

GEPs are typically circulated by the heat carrier fluid inside the pile. The most common heat transfer fluid (HTF) is water, H_2O. It is selected for its good heat transfer performance and the vast majority of desirable properties, such as high heat capacity, low viscosity, high inflammability and nontoxicity [15-21]. Analysis on the lifetime of water energy extraction system proposed by Cao, Huang and Jiang [22] confirms the popularity of water as HTF. However, one typical drawback associated with the usage of water in energy exchanger is the high freezing point [23,24]. To increase the reliability of water in heat exchanger, additives are recommended to solve the freezing issue in practical projects [25,26], which was initially raised by O'Dell, Mitchell and Beckman [27]. Only in the past twenty years have studies described the role of **sCO** $_2$ as HTF. Early examples of research into sCO_2 can be referred to Pruess [28] and Brown [29]. One significant advantage of sCO_2 over water is that it avoids the problem of high freezing point [30,31]. Compared to water which can be only operated in an above-zero-degree condition, sCO_2 provides more mobility, allowing system operated in winter. Another advantage of using sCO_2 is that it allows the same or even higher rate of energy extraction [29,22,32,33]. Besides, desirable properties of CO_2 can be deliberated by the control of pressure [34]. The thermophysical properties of H_2O are only sensitive to temperature, while those of CO_2

* Corresponding author.
E-mail address: yixiang.gan@sydney.edu.au (Y. Gan).

https://doi.org/10.1016/j.deepre.2025.100169
Received 14 November 2024; Received in revised form 19 February 2025; Accepted 20 February 2025
Available online 24 March 2025

are sensitive to both temperature and pressure [35]. Such unique properties of CO_2 allow controlling GEP circulating pipe in a tuneable way. However, there are limited systematic studies focusing on demonstrating the advantages of CO_2 when compared to H_2O at various operational conditions.

Although experimental, numerical or analytical methods have been encountered in previous publications on GEPs, most of them focus on identifying and evaluating the operative condition and design configuration [36-38]. However, several aspects of HTF remain to be extensively discussed. This study aims to address the influence of CO_2 as a new HTF on GEPs by comparing different HTFs using a newly introduced evaluation criterion. This study simulates the daily operation of GEPs in winter (cooling mode) and the associated scientific and engineering challenges by providing numerical analysis of sCO_2 as HTF. As a result of the analysis presented in this work, a thermal performance evaluation for energy piles is proposed by the Ragone plot.

2. Method

2.1. System characterisation

Fig 1 shows the 2D numerical axisymmetric model extracted from the 3D real case, for the sake of simplicity in simulating heat exchange process. Therein, the coaxial tube is surrounded by soils. Besides, the design of the model geometry is based on the real size of GEPs, of which the main parameters are listed in Table 1. The annuli pipe with the same inlet and outlet area is chosen in this study.

Reflecting the discharge energy of the battery at different power levels, Ragone plot combines the storage capacity and power supply capability of the battery into a curve. The diagram generated from theory of Ragone plot clearly describes the trade-off between energy and power and can also reflect the best working area of certain system. Additionally, the Ragone plot is used to compare the performance of various energy storage devices. As a new concept applied in the heat exchange system, Ragone plot is the curve of the specific energy versus power to evaluate GEPs system. The cutoff temperature, T_{cutoff}, is commonly introduced to investigate the thermal performance. By assuming different values of T_{cutoff}, the temperature difference and the cutoff effectiveness can be expressed as

$$\Delta T = T_0 - T_{\text{cutoff}}, \tag{1}$$

$$\eta = \frac{T_{\text{in}} - T_{\text{cutoff}}}{T_0 - T_{\text{in}}}, \tag{2}$$

where ΔT is temperature difference, T_0 is the initial temperature of soil, η is cutoff effectiveness, T_{in} is the fluid temperature at inlet. The constraint $T_{\text{cutoff}} = T_{\text{out}}$ is adopted, where T_{out} is the fluid temperature at outlet.

Table 1
GEP control parameters.

Property		Value
r_i	Inner tube inner diameter	6 cm
r_o	Inner tube outer diameter	2.22 cm
d_s	Thickness of tube layer	1 cm
R_o	Outer tube outer diameter	10.22 cm
L_i	Length of inner tube	11.93 m
L	Length of the single GEP	12 m
l_x	Half length of surrounding soil x direction	1.635 m
L_z	Depth of surrounding soil z direction	13.53 m
ρ_w	Density of pipe	7850 kg/m^3
C_{pw}	Heat capacity of pipe	475 J/(kg °C)
k_w	Thermal conductivity of pipe	44.5 W/(m °C)
h_{add}	Additional heat exchange coefficient	2000 W/(m^2 °C)

The extracted energy, E, and average power, q, which are utilised to evaluate GEP via Ragone plot, are summarised in Table 2. Prior to commencing the Ragone plot study, the change of temperature over time, T–t, and the change of power over time, q–t, are directly sought from the numerical model. After introducing a specific T_{cutoff}, the respective cutoff time could be extracted from the T–t plot. The cutoff time is then implemented into q–t to find the respective cutoff power. Finally, the extracted energy of GEP is accumulated, which is calculated by integrating the cutoff power within the cutoff time. The time interval for cutoff, Δt, is defined as

$$\Delta t = t_{\text{cutoff}} - t_0, \tag{3}$$

where t_0 is the time when HTF fluid at inlet reaches the outlet region, t_{cutoff} is the corresponding time when the temperature of outlet reaches T_{cutoff}.

Pareto front, reflecting the optimal solution under multi-objective

Table 2
Properties and definitions for electrochemical, thermal storage and geothermal energy piles system.

	Electrochemical storage	Phase change thermal storage	GEPs
Ideal input	Open-circuit voltage (V)	Transition temperature (K)	Soil cutoff temperature (°C)
Discharge current or power	$I = \frac{\Delta V}{R_e}$ (A)	$\dot{q} = \frac{\Delta T}{R_{\text{th}}}$ (W)	$q = \frac{E}{\Delta t}$ (W)
Energy	$E = \int I dt$ (Ah)	$E = \int \dot{q} dt$ (Wh)	$E = \int q dt$ (W s)

*The definition for electrochemical storage and phase change thermal storage are adopted from Woods, Mahvi, Goyal, Kozubal, Odukomaiya and Jackson [39].

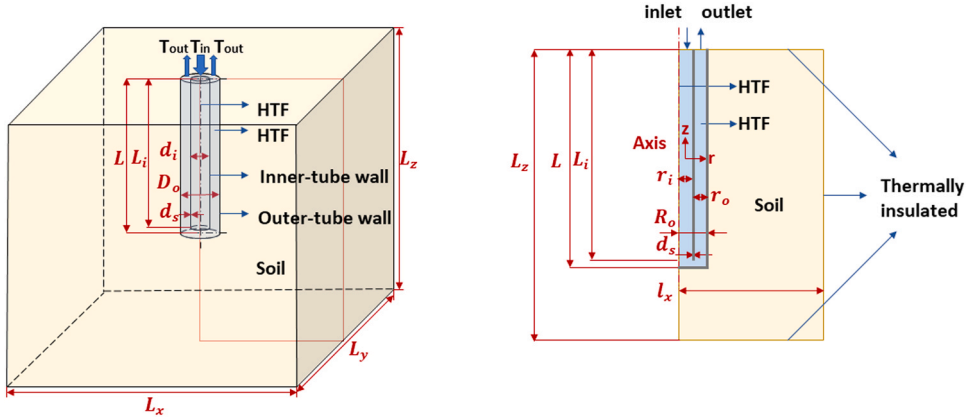

Fig. 1. GEPs model: 3D concentric tube with surrounding soil (left) and 2D axisymmetric simplified model (right).

problem, is adopted to estimate the optimal operation condition and define the proper operation region under different cutoff temperatures. The relation between q and E is fitted in the superellipse form,

$$E = \left(1 - \left(\frac{q}{q_0}\right)^c\right)^{\frac{1}{c}} \cdot E_0, \tag{4}$$

$$\left(\frac{E}{E_0}\right)^c + \left(\frac{q}{q_0}\right)^c = 1, \tag{5}$$

where c is a fitting parameter.

2.2. Numerical model

To conduct the numerical analysis, the computational fluid dynamics (CFD) with forced convection of HTF and heat transfer model in it are adopted. The core module in COMSOL Multiphysics 5.6 is employed to solve one physical model problem using consistent variables among different physical fields. The heat transfer model is involved to imitate the heat convection and heat conduction between HTF and the tube, where the velocity field is coupled. Besides, the heat transfer in solid is also analysed based on the heat conduction between tube and soil domain.

Non-isothermal compressible flow conjugated with heat transfer is typically solved based on main formulations of continuity, momentum and energy equations, which are expressed as

$$\frac{\partial \rho}{\partial t} + \nabla \cdot (\rho u) = 0 \tag{6}$$

$$\rho \frac{\partial u}{\partial t} + \rho u \cdot \nabla u = -\nabla p + \nabla \cdot (\mu(\nabla u + (\nabla u)^T) - \frac{2}{3}\mu(\nabla \cdot u)I) + F + \rho g \tag{7}$$

$$\rho C_p u\left(\frac{\partial T}{\partial t} + u \cdot \nabla T\right) + \nabla \cdot (-k \nabla T) = \alpha_p T\left(\frac{\partial p}{\partial t} + u \nabla p\right) \tag{8}$$

The applied turbulent model $k-\varepsilon$, to investigate flow performance in GEPs with sCO_2 as HTF, and the viscosity are represented as

$$\mu_T = \rho C_\mu \frac{k^2}{\varepsilon} \tag{9}$$

$$k = \frac{3}{2}(|U| I_T)^2 \tag{10}$$

$$\varepsilon = C_\mu^{\frac{3}{4}} \frac{k^{\frac{3}{2}}}{L_T} \tag{11}$$

The pipe wall supports the heat transfer in solid media, where the total effective thermal conductivity is described as

$$k_{tot} = \frac{\sum_n \frac{k_n}{d_n}}{\sum_n d_n}, \tag{12}$$

where k_{tot} is the equivalent thermal conductivity considering all thermal layers, n is the number of the layer, k_n is the specific thermal conductivity of each layer, and d_n is the specific thickness of each layer.

The tube material is selected as the structural steel from the default embedded material bank, which is assumed to have enough strength to maintain the operating pressure. Moreover, the underground soil is assumed to be fully saturated, of which the detailed properties are listed in Table 3.

2.3. Model validation for sCO_2 database

To validate the model, model reliability on supercritical fluid properties and the data accuracy in numerical simulations on heat transfer are involved. GEPs are normally installed vertically to extract more geothermal energy. The gravity effect and buoyancy effect will be applied along the whole vertical pipe flow. Therefore, the vertically built tube is chosen as the filter in model validation, of which the experiment study is based on Jiang, Xu, Lv, Shi, He and Jackson [42], focused on the heat transfer of sCO_2 in a vertical tube. To validate sCO_2 in numerical simulation, a single concentric cylinder is selected as the model geometry for the parameter validation. In Fig. 2, the 3D experimental equipment is simplified into a 2D axisymmetric model.

Table 3
Underground soil properties.

Property		Value
S	Degree of saturation	1
ρ_s	Dry density of soil	1450 kg/m^3
ρ_f	Density of pore fluid	997 kg/m^3
ρ_b	Bulk density of soil, $\rho_b = \rho_s + \frac{e \cdot S \cdot \rho_w}{1+e}$	2063 kg/m^3
k_b	Thermal conductivity of soil	1.5 W/(m °C)
k_f	Thermal conductivity of pore fluid	0.022 W/(m °C)
$C_{p,b}$	Specific heat of soil	1269 J/(kg °C)
$C_{p,f}$	Specific heat of pore fluid	4182 J/(kg °C)
γ_{p_f}	Specific heat ratio of pore fluid	1
e	Initial void ratio	1.6
n	Porosity, $n = \frac{e}{1+e}$	0.615

*The properties of pore fluid are adopted from Lemmon, Huber and McLinden [40]. The bulk properties of soil and the dry density of soil are adopted from Nguyen, Wu, Gan, Pereira and Tang [41].

The properties of sCO_2 in Fig. 3 are generated based on the standard of National Institute of Standards and Technology (NIST). Geometry details and tube material properties are listed in Table 4.

To validate the numerical simulation by the corresponding experimental data, several boundary conditions about temperature, pressure, mass flux and heat flux are considered. Firstly, the temperature detected from the thermocouple is linearly increased, which is imported as the temperature boundary condition along the tube wall. The inlet temperature T_{in} is set to be 51°C, and other parts of the pipe are thermal insulated. Secondly, a velocity-control sCO_2 flow at the inlet and a pressure-control at the outlet are selected. The mass flow rate, $\dot{m}$, at the inlet is set to be 1.47 kg/h. The outlet pressure, P_{out}, is set to be 9.4986 MPa, enabling to keep the inlet pressure of the system at 9.5 MPa [42]. The experiment system was insulated thermally, and the thermocouples, connected with the tube surface, reflect the temperature of the wall surface. Furthermore, for the same heat flux on the inner tube surface, an extra thin layer is inserted, and the average heat flux q_w through the inner tube surface is 31 kW/m^2. With the equivalent heat transfer coefficient k_w, and the additional heat transfer coefficient h_{add}, the theoretical wall heat exchange rate h_w is expressed as

$$h_w = \frac{1}{\frac{1}{h_{add}} + \frac{d_s}{k_w} + \frac{1}{h_{add}}}, \tag{13}$$

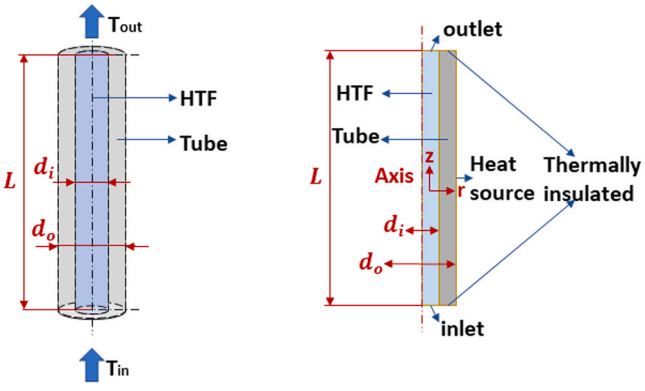

Fig. 2. Schematic of sCO_2 validation model: 3D experimental concentric unit (left), and 2D axisymmetric simplified model (right).

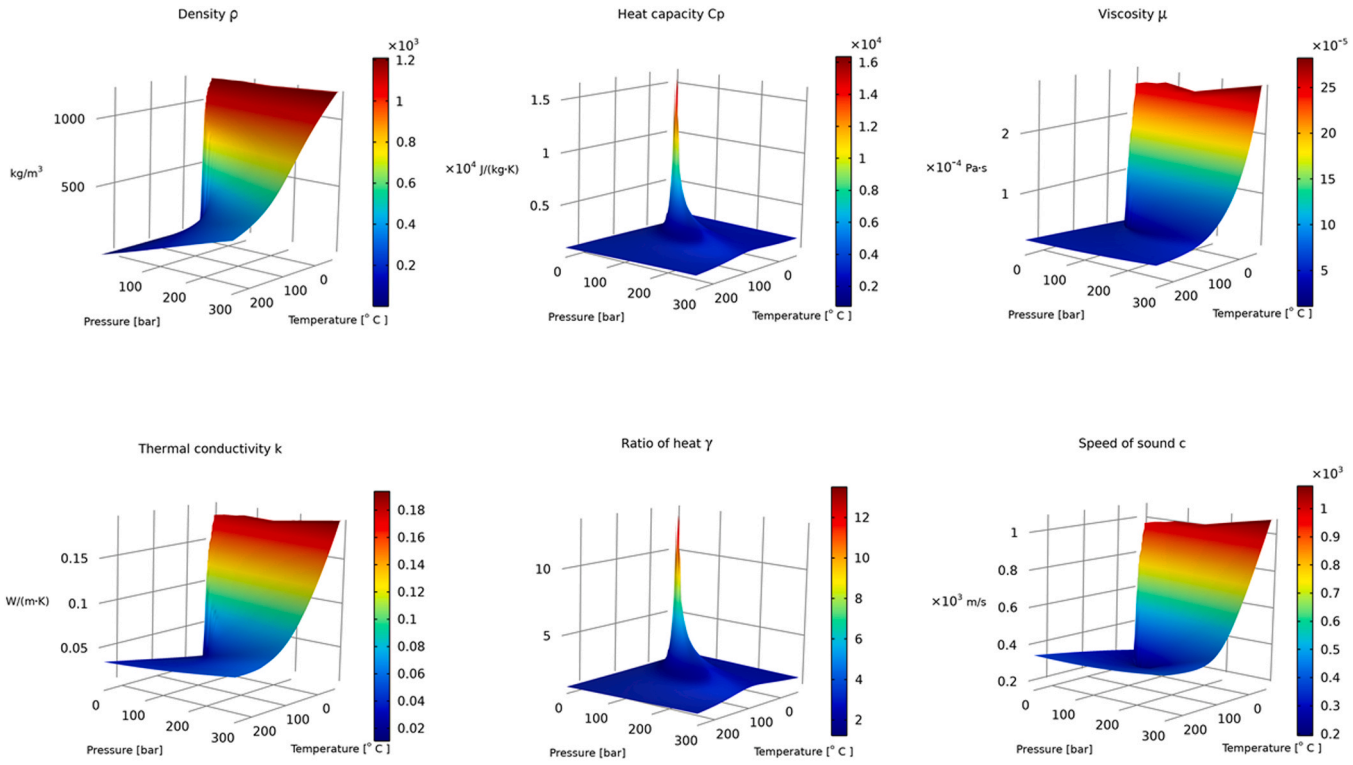

Fig. 3. The sCO_2 properties plotted by COMSOL, including density 2° kg/m^3, heat capacity at constant pressure C_{pCO_2} J/(kg °C), dynamic viscosity μ_{CO_2} N s/m^2, thermal conductivity k_{CO_2} W/(kg °C), specific heat ratio $\gamma(\gamma = C_{pCO_2}/C_{vCO_2})$, sound speed inside sCO_2c m/s.

Table 4
Validation parameters.

Property		Value
d_o	Inner tube outer diameter	17.29×10^{-4} m
d_i	Inner tube inner diameter	9.48×10^{-4} m
L	Length of pipe	55 mm
ρ_w	Density of pipe	8000 kg/m^3
C_{pw}	Heat capacity of pipe	500 J/(kg °C)
k_w	Thermal conductivity of pipe	16.5 W/(m °C)
h_{add}	Additional heat transfer coefficient	7142 W/(m^2 °C)

which is equal to 3920 W/(m^2 °C).

The numerical results of sCO_2 heat transfer in pipe flow are plotted in Fig. 4. For flow with heat transfer, model validation usually utilises a temperature field to explore the result of heat exchange efficiency in pipe flow. In the left subfigure of Fig 4, the wall temperature is set according to the linear fitting of experimental data. The fluid temperature, T_f, keeps 51 °C at the inlet. When CO_2 flows up and absorbs heat flux from the inner tube surface, the fluid temperature increases along the tube. The extracted energy flux from the tube is about 31 kW/m^2 on average, while q_w is consistent with the magnitude in the experiment. The local heat transfer coefficient, calculated from q_w and local temperature difference, decreases, due to the thermal resistance and the uneven properties distribution of thermal properties among the fluid cross-sectional area.

2.4. The setting of parametric studies

A well-structured model with suitable mesh sizes is required to secure the simulation accuracy. Five structural mesh sizes are selected to perform the mesh size sensitivity study, as shown in Fig. 5; therein, the

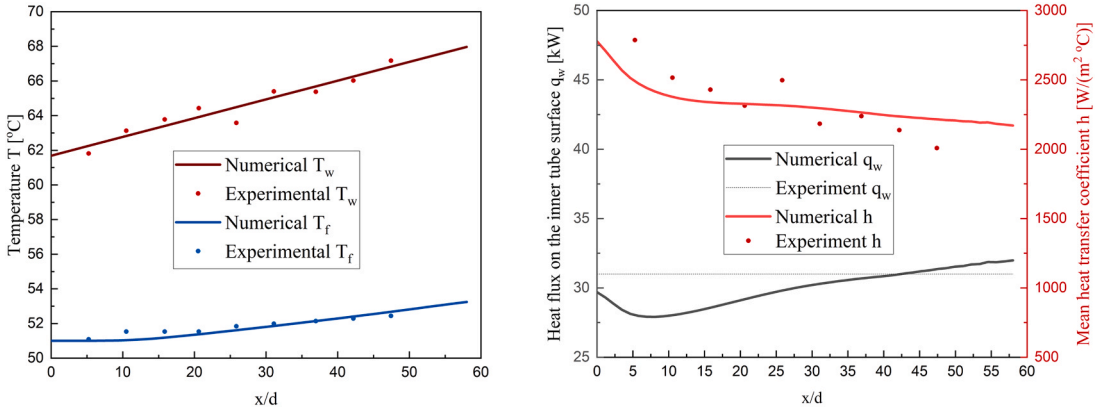

Fig. 4. Validation results along the tube, where d = 0.948 mm, $\dot{m}$ = 1.47 kg/h, P_0 = 9.5 MPa, q_w = 31 kW/m^2: Heat flux on the inner tube surface q_w and local heat transfer coefficient h (left). Wall and fluid temperature distribution (right).

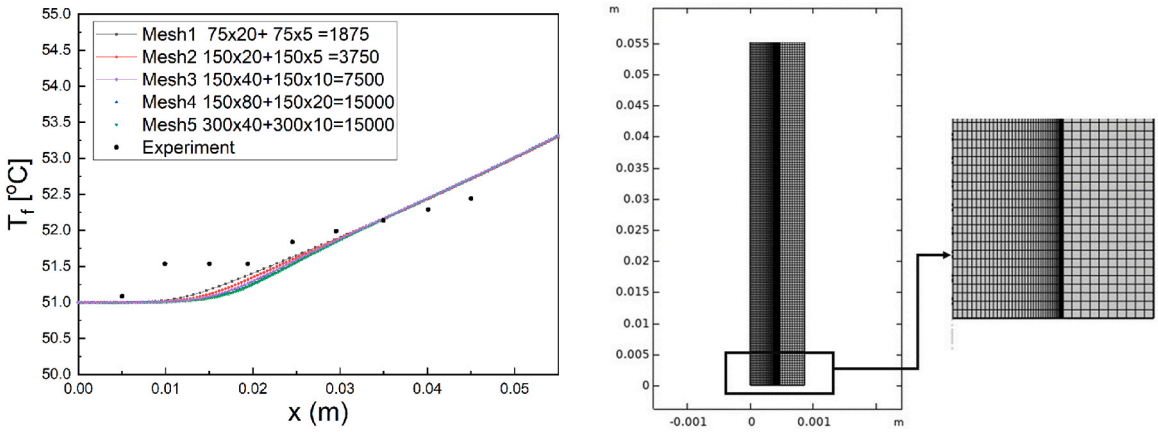

Fig. 5. Mesh sensitivity study and selection: Bulk fluid temperature at location x(m) along tube length under different mesh sizes (left). Mesh selection of the FEM (right).

mesh number of these meshes are also provided. Except for the outer boundaries of the HTF are split by graded fine meshes, the tube and the inner parts of the HTF are meshed with uniformly quadrangular meshes. Evidently, 7500 meshes in Mesh 3 are fine enough to achieve a balance between the simulation accuracy and the computation consumption.

To simplify the model, the initial temperature of the whole system, including single GEP and soil domain, is assumed to be 15 °C regardless of the depth. Regarding boundary conditions, the temperature, the inlet velocity, and outlet pressure are the main dominant parameters in this model. The temperature of inlet fluid 5 °C is used to simulate the winter temperature. The boundaries of the soil domain and the top edges of the tube are set to be thermal insulated and not affected by the ambient temperature.

The HTF flow is velocity-control at the inlet. Pressure at the outlet in the CO_2 GEP is set as 85 bar to avoid the phase change. The phase change around critical points leads to a significant change in thermo-physical properties, which might further cause a non-stable pipe flow. To mitigate this impact, this study adjusts pressure and temperature to keep CO_2 in the supercritical state. Additionally, since the single GEP is installed vertically into the soil domain, gravity needs to be taken into account. The backflow is not allowed at the outlet. All wall interfaces are assumed to be non-slip. Finally, energy loss caused by the collision between fluid and tube wall at the bottom corner of annuli, in terms of the kinetic energy loss inside the single GEP is assumed to be ignored. A proper thermal-insulated strategy, such as an additional thermal baffle or a dummy pile, will play an essential role in addressing the issue of heat exchange reduction. To simulate the influence of thermal insulation, an additional heat exchange coefficient, h_{add}, is adopted to mitigate the effect of thermal interference between inlet and outlet, where h_{add} is applied on the surface of the inner tube. In Eq. (13), heat exchange coefficient h_{add} is required to count twice because the thermal-protective coating is applied on both sides of the inner tube.

Based on the boundary conditions mentioned above, the percentage of cutoff η and respective T_{cutoff} are summarised in Table 5.

Table 5
Cutoff effectiveness and corresponding cutoff temperature.

η	T_{cutoff} (°C)
10 %	6
30 %	8
50 %	10
70 %	12
90 %	14

3. Results and discussions

3.1. Thermal performance of GEPs

In Table 6, CO_2 GEP and H_2O GEP, corresponding to different HTFs, are involved; the comparison of various HTF has been assessed using the Péclet number considering both operation inlet velocity and HTF properties. When the Reynolds number is greater than 3500, the pipe flow is normally treated as turbulent flow. Laminar flow exists when the value of Reynolds number is less than 2000. Hence, only the inlet velocities corresponding to Reynolds numbers below 2000 and above 6000 are considered in H_2O GEP studies, which could avoid the transitional flow which is non-trail to be considered in current CFD scheme.

Fig 6 represents the results obtained from the respective preliminary analysis on thermal performances of CO_2 and water GEPs. This figure is quite revealing in several ways. Firstly, the relationship T–t in the right three diagrams identifies the influence of inlet flow velocity on the heat exchange process in the entire system. The T_{in}, approximately maintained at 15 °C, records the highest temperature, then the fluid bulk temperature starts to drop over time. This is because the temperature variation between the pile and surrounding soil leads to the reduction of heat exchange efficiency. Secondly, CO_2, which indicates lower levels of inlet velocity under the similar Péclet number, indicating higher levels of fluid bulk temperature than water. We can infer that CO_2, having more time to flow inside GEP, will absorb more energy, and therefore the decreasing rate of temperature over time is not as great as that of water.

The left three plots in Fig. 6 represent the $q-t$ relationship, which is more concerned with fluid properties. The trend of $q-t$, while

Table 6
Groups of GEP with different HTF, CO_2 and H_2O, under the similar magnitude of Péclet number.

Group	Group 1		Group 2		Group 3	
	CO_2	H_2O	CO_2	H_2O	CO_2	H_2O
v (m/s) inlet vl.	0.005	0.009	0.04	0.1	0.4	1
Re Reynolds nr.	5510	714.0	44,080	7933	440,800	79,340
Pr Prandtl nr.	2.1×10^{-3}	1.11×10^{-2}	2.1×10^{-3}	1.1×10^{-2}	2.1×10^{-3}	1.1×10^{-2}
Pe Péclet nr.	11.57	7.930	92.56	88.13	925.6	881.3
Range of *Pe*	$Pe \in [1,20]$		$Pe \in [20,100]$		$Pe \in [100,1000]$	

*In the first column, *vl.* is used as a written abbreviation for velocity, *nr.* is the abbreviation for number.

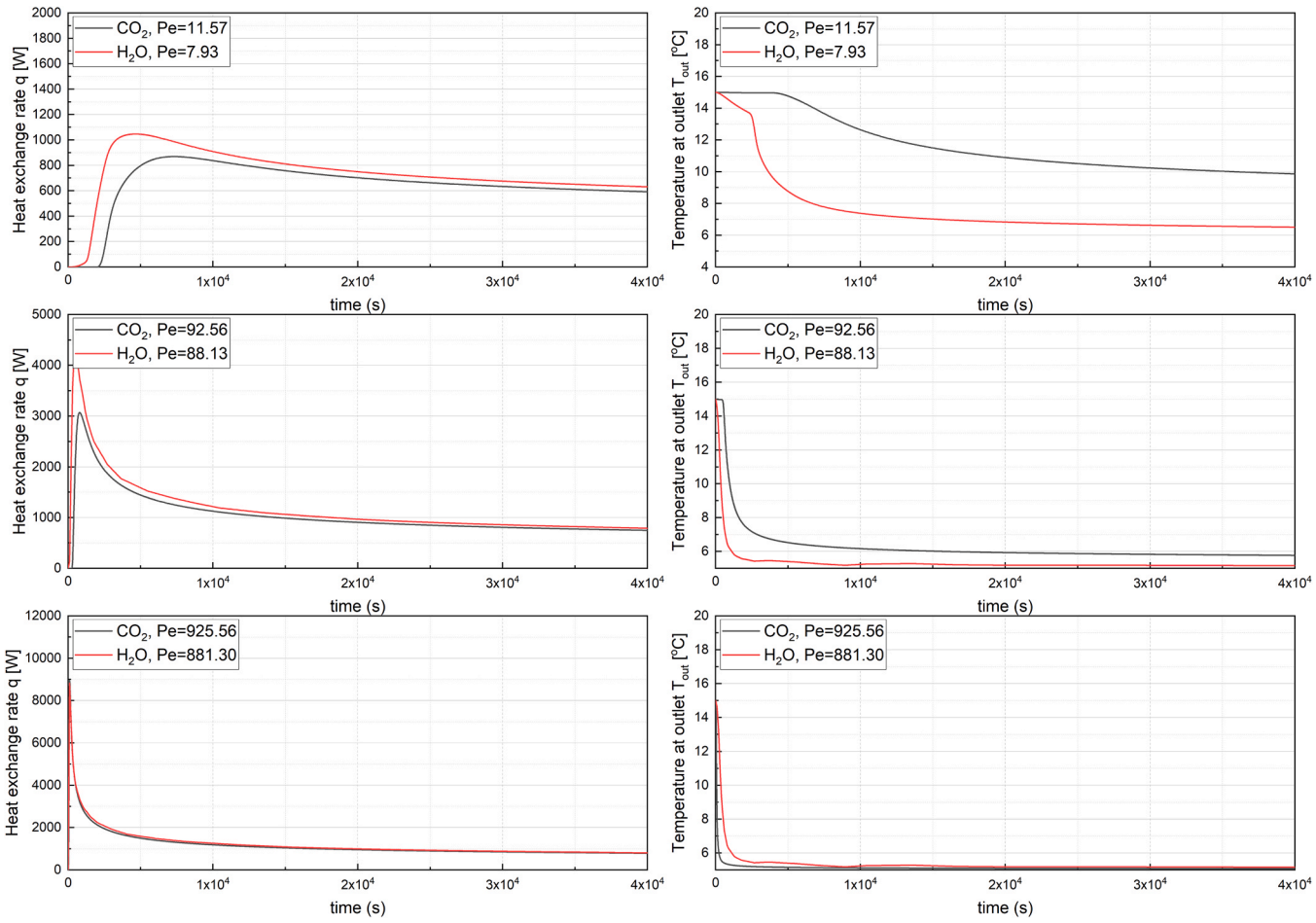

Fig. 6. Comparative thermal performance results of sCO_2 (black) and H_2O (red) in the GEP system, respectively for low Péclet number ($Pe \in [1,20]$), intermediate Péclet number ($Pe \in [20,100]$), high Péclet number ($Pe \in [100,1000]$). The left three diagrams show the relationship of heat extraction rate (q) over time, and the right three diagrams show temperature at outlet (T_{out}) change over time.

preliminary, suggests that less energy is stored in the entire system. This is because more energy is extracted over time and the heat exchange rate gradually decreases. Additionally, $q-t$ also suggests that the peak power of H_2O GEP is higher than that of CO_2, where the discrepancy could be attributed to the properties of HTF. The power q and Péclet number Pe are closely linked, which are respectively written as

$$q = C_p \rho v \left(\frac{1}{4}\pi\right) D^2 \Delta T \tag{14}$$

$$Pe = \frac{C_p \rho v L}{k} \tag{15}$$

where C_p is HTF specific heat, ρ is HTF density, v is HTF inlet velocity, k is HTF thermal conductivity, D and L are diameter and length of tube, ΔT is temperature difference and identified in Eq. (1)

These two equations can be further associated as

$$q = Pe \cdot k \cdot \Delta T \frac{\frac{1}{4}\pi D^2}{L}, \tag{16}$$

where $\frac{\frac{1}{4}\pi D^2}{L}$ is a constant value under the same geometry of GEP. Under a similar Péclet number with the same T_{cutoff}, the peak power will benefit from thermal conductivity, where the water typically has a higher thermal conductivity than CO_2.

3.2. Ragone plot evaluation on CO_2 and water

The Ragone plot could further evaluate the overall heat exchange performance under different T_{cutoff}. We take Group 2 under the cutoff temperature 10 °C as an example to better explain the form of the Ragone plot. By comparing CO_2 and H_2O in Group 2, CO_2 takes longer to reach 10 °C, which leads to a relatively lower average power but a higher total extracted energy. This finding is proved by the marked points in Fig. 7. For the purpose of estimation on other operation ranges, all analyses are carried out using the same way.

Fig 7 firstly presents that the points on the Ragone plot are projected to shift upper left with the increasing Péclet numbers. With a shorter running time inside GEP under high inlet Péclet numbers, HTF will bring out less energy than those of low Péclet numbers. Secondly, Fig. 7 demonstrates that sCO_2-based GEP systems achieve higher power output and greater extracted energy than H_2O-based GEP systems. The thermal performances of CO_2 and water are comparable in high Péclet number scenarios, while CO_2 cases are significantly different from those of H_2O in low Péclet numbers.

For $T_{cutoff} = 10$ °C, to meet the same energy demand, the CO_2 GEP could provide 1.5–4 times the power efficiency to that of water. Under the same operation power, CO_2 GEP achieves 4–10 times the energy density than that of water. These findings underscore the thermodynamic benefits of CO_2, particularly in low Péclet number scenarios where its enhanced heat transfer properties play a crucial role. Fig. 7 also reveals that, as the growth of T_{cutoff}, the thermal performances of CO_2 become significantly different from those of H_2O. The increase of

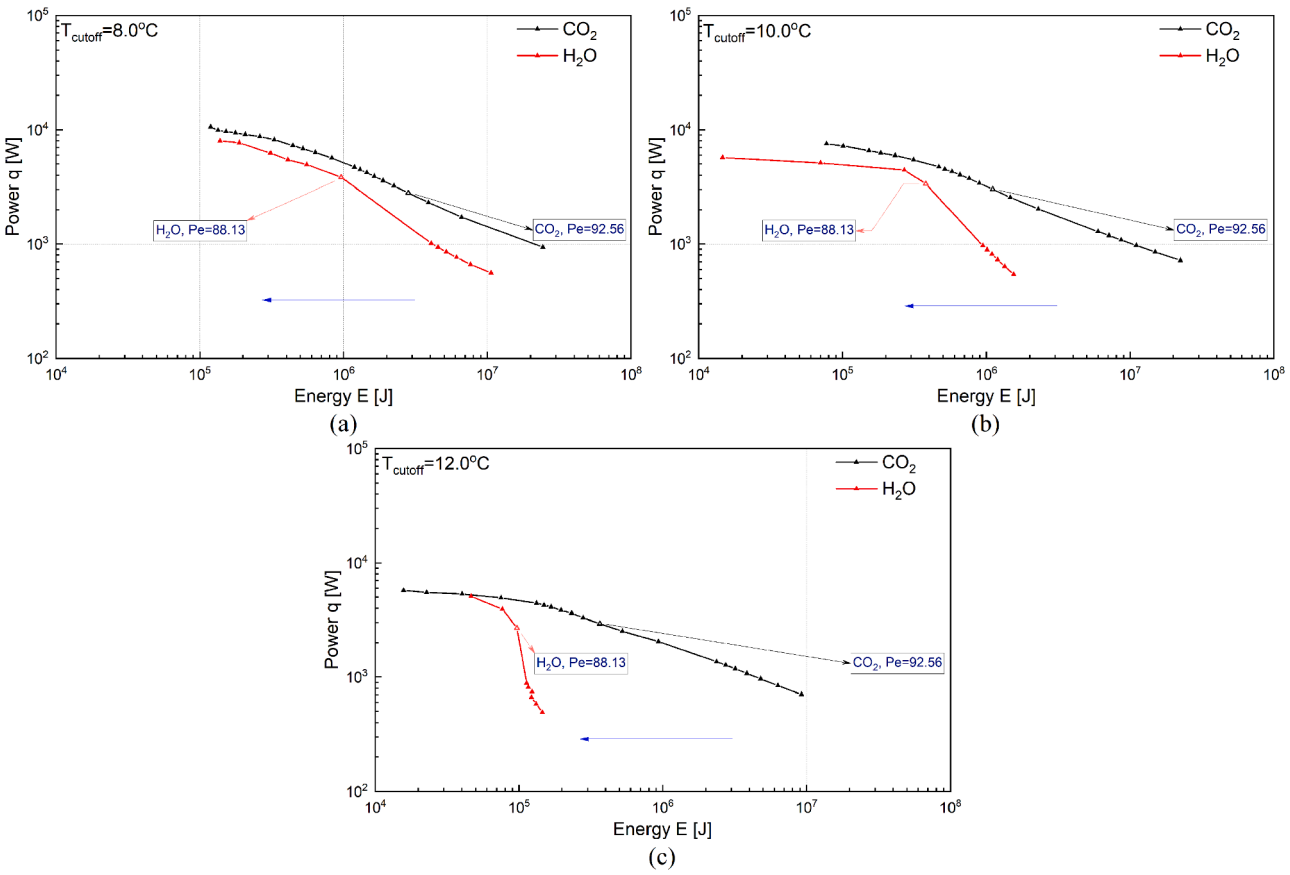

Fig. 7. Ragone plot for the GEP using CO_2 and water (corresponding to black and red curves) as geothermal fluids with different cutoff temperatures: (a) $T_{cutoff} = 8.0$ °C, (b) $T_{cutoff} = 10.0$ °C, (c) $T_{cutoff} = 12.0$ °C. The blue arrow indicates the direction of increasing inflow Péclet number for each specific line.

T_{cutoff} contributes to the decrease of desired energy, meanwhile, it maintains the high η and system power within a short time.

3.3. Ragone plot evaluation on CO_2 system combining Pareto front

For the purpose of finding optimal solutions for the Ragone plot in the marginal area, Pareto fronts are introduced with various fitting functions. In Fig. 8, the potential extracted energy and maximum power could be acquired via the intersections of the x-axis and y-axis, respectively. With the growth of T_{cutoff}, both potential energy and the maximum power will accordingly increase. To control bias, curve fittings for Ragone plots are also carried out from the superellipse form. Similar trends of E_0, q_0 between the two groups are evident despite the differences among actual magnitudes.

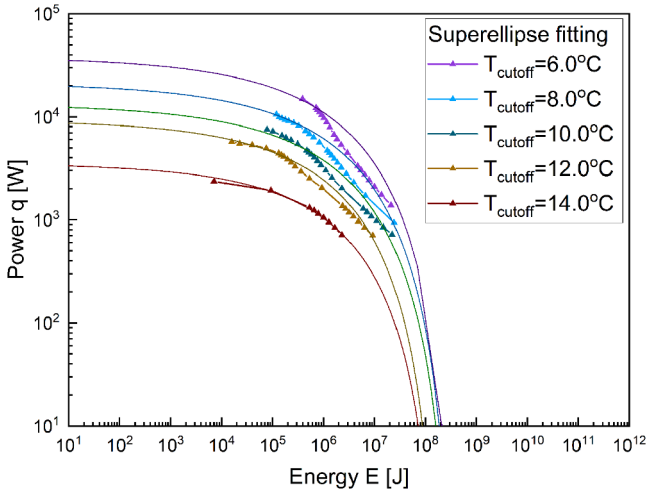

Fig. 8. Ragone plot for the GEP using CO_2 as geothermal fluids with Pareto fronts employing superellipse curve fitting.

Table 7 summarises data sets of E_0,q_0 collected from superellipse fitting function. The results of the correlational analysis on fitting function could be summarised that the larger potential energy will accordingly obtain a smaller maximum power. This observation could conceivably support the hypothesis of Pareto fronts that any increases in one objective will cost the other decrease in a multi-objective scenario.

4. Conclusions

This study on GEPs is numerically investigated by FEM, with the main aims: (1) to examine the data accuracy of the utilisation of CO_2 in the supercritical state as HTF, and (2) to assess the comparable heat exchange performance between water and CO_2 inside GEPs. The insights gained from this study are summarised below:

Table 7
Estimated maximum potential energy, E_0, maximum heat exchange rate, q_0, and the coefficient of determination R^2 under curve fitting function in several cutoff temperatures.

T_{cutoff} (°C)	E_0 (J)	q_0 (W)	R^2
6	2.85×10^8	3.63×10^4	0.827
8	2.67×10^8	2.04×10^4	0.875
10	2.41×10^8	1.27×10^4	0.906
12	1.31×10^8	8.95×10^3	0.944
14	1.18×10^8	3.41×10^3	0.994

- Ensuring appropriate systems, support for the sCO_2 database should be a priority. As reliable predictors in heat transfer, the fluid temperature, T_f, and heat transfer coefficient, h, show the same trend and similar magnitude as the experimental study. The model reliability study suggests that the accurate heat transfer model could be achieved through the sCO_2 dataset.
- For the comparison study, the coaxial-shaped GEPs circulated by CO_2 and water are investigated under similar Péclet numbers. The investigation identified that CO_2 has a better heat exchange performance than water in the GEP, where CO_2 GEP could provide 4 times the power efficiency and 10 times the energy density than that of water under the certain operating condition.
- The view of the Péclet number proves instructive in expanding the understanding of how the HTF will influence the thermal performance of GEP. Also, the Ragone plot emerges as a reliable predictor of system overall heat exchange performance.

The model validation clearly supports the employment of sCO_2 on heat exchange performance. Then, the results of this research provide insights for sCO_2 feasibility as HTF in the GEP. The findings of this study reveal that sCO_2's exceptional thermal properties, such as higher energy density and heat transfer efficiency, position it as an optimal HTF for geothermal energy piles in compact or high-energy-demand environments. However, water remains a practical and cost-effective alternative for regions with milder climates or applications with lower operational pressures. By tailoring HTF selection to site-specific climatic and geological conditions, feasibility research on GEP systems for local region can be considered and this insight provides a framework for optimizing GEP designs, operational efficiency in a wide range of real-world scenarios.

CRediT authorship contribution statement

Linxiao Zhou: Writing – original draft, Visualization, Investigation, Formal analysis, Data curation. **Haobin Liang:** Writing – review & editing, Validation, Software, Investigation. **Deheng Wei:** Writing – review & editing, Validation. **Yixiang Gan:** Writing – review & editing, Supervision, Software, Resources, Project administration, Methodology, Funding acquisition, Conceptualization.

Declaration of Competing Interest

The authors declare that they have no known competing financial interests or personal relationships that could have appeared to influence the work reported in this paper.

References

[1] R. Cunha, P. Bourne-Webb, A critical review on the current knowledge of geothermal energy piles to sustainably climatize buildings, Renew. Sustain. Energy Rev. 158 (2022) 112072.
[2] Z. Liu, Y. Zhou, J. Yan, M. Tostado-Véliz, Frontier ocean thermal/power and solar pv systems for transformation towards net-zero communities, Energy 284 (2023) 128362.
[3] S.M. Lu, A global review of enhanced geothermal system (egs), Renew. Sustain. Energy Rev. 81 (2018) 2902–2921.
[4] Y. Zhou, Z. Liu, A cross-scale 'material-component-system' framework for transition towards zero-carbon buildings and districts with low, medium and high-temperature phase change materials, Sustain. Cities Soc. 89 (2023) 104378.
[5] Z. Liu, Y. Sun, C. Xing, J. Liu, Y. He, Y. Zhou, G. Zhang, Artificial intelligence powered large-scale renewable integrations in multi-energy systems for carbon neutrality transition: challenges and future perspectives, Energy AI 10 (2022) 100195.
[6] K. You, Y. Yu, W. Cai, Z. Liu, The change in temporal trend and spatial distribution of co2 emissions of china's public and commercial buildings, Build. Environ. 229 (2023) 109956.
[7] Loveridge, F.A., Powrie, W., 2016.The average temperature of energy piles, In: Geo-Chicago 2016, pp. 66–175.
[8] J. Lund, B. Sanner, L. Rybach, R. Curtis, G. Hellström, Geothermal (ground-source) heat pumps: a world overview, Geo-Heat Cent. Q. Bull. (2004) 25.
[9] S.q. Cui, C. Zhou, J.q. Liu, D.B. Akinniyi, Stress effects on thermal conductivity of soils and heat transfer efficiency of energy piles in the saturated and unsaturated soils, Comput. Geotech. 160 (2023) 105549.
[10] A. Khalil, M. Attom, Z. Khan, P.V. Astillo, O.M. El-Kadri, Recent advancements in geothermal energy piles performance and design, Energies 17 (2024) 3386.
[11] L.B. Neto, G. Narsilio, N. Makasis, R. Choudhary, Y. Carden, Experimental and numerical data of thermal response tests executed in groups of energy piles connected in series, Data Brief. 48 (2023) 109256.
[12] Y. Zhou, S. Zheng, Z. Liu, T. Wen, Z. Ding, J. Yan, G. Zhang, Passive and active phase change materials integrated building energy systems with advanced machine-learning based climate-adaptive designs, intelligent operations, uncertainty-based analysis and optimisations: a state-of-the-art review, Renew. Sustain. Energy Rev. 130 (2020) 109889.
[13] Z. Mohamad, F. Fardoun, F. Meftah, A review on energy piles design, evaluation, and optimization, J. Clean. Prod. 292 (2021) 125802.
[14] M.E. Zayed, J. Zhao, W. Li, A.H. Elsheikh, A.M. Elbanna, L. Jing, A. Geweda, Recent progress in phase change materials storage containers: geometries, design considerations and heat transfer improvement methods, J. Energy Storage 30 (2020) 101341.
[15] Z. AlHajaj, M.Z. Saghir, Numerical study on the influence of embedded pcm tubes on the energy storage properties of the geothermal energy pile, Int. J. Thermofluids 20 (2023) 100416.
[16] S. tenBosch, E. Ravera, L. Laloui, Performance of energy piles foundation in hot-dominated climate: a case study in dubai, Renew. Energy 220 (2024) 119632.
[17] Z. Chen, X. Lian, J. Tan, H. Xiao, Q. Ma, Y. Zhuang, Study on heat-exchange efficiency and energy efficiency ratio of a deeply buried pipe energy pile group considering seepage and circulating-medium flow rate, Renew. Energy 216 (2023) 119020.
[18] M. Daneshipour, R. Rafee, Nanofluids as the circuit fluids of the geothermal borehole heat exchangers, Int. Commun. Heat Mass Transf. 81 (2017) 34–41.
[19] J. Gong, K. Sumathy, Active solar water heating systems, in: Advances in Solar Heating and Cooling, Elsevier, 2016, pp. 203–224.
[20] H. Narei, R. Ghasempour, Y. Noorollahi, The effect of employing nanofluid on reducing the bore length of a vertical ground-source heat pump, Energy Convers. Manag. 123 (2016) 581–591.
[21] Z. Wang, Design of Solar Thermal Power Plants, Academic Press, 2019.
[22] W. Cao, W. Huang, F. Jiang, Numerical study on variable thermophysical properties of heat transfer fluid affecting egs heat extraction, Int. J. Heat Mass Transf. 92 (2016) 1205–1217.
[23] S. Mellari, Experimental investigation and modeling of the pressure drop of ice slurry flow in horizontal pipe, Int. J. Refrig. 147 (2023) 134–142.
[24] J. Westhaeuser, L. Brauchle, J.C. Albrecht, W. Tegethoff, N. Lemke, J. Koehler, Flat tube heat exchangers: experimental analysis of frosting and water retention, Appl. Therm. Eng. 218 (2023) 119319.
[25] H. Babar, H. Wu, W. Zhang, T.R. Shah, D. McCluskey, C. Zhou, The promise of nanofluids: a bibliometric journey through advanced heat transfer fluids in heat exchanger tubes, Adv. Colloid Interface Sci. (2024) 103112.
[26] K. Natesan, S. Karinka, A comprehensive review of heat transfer enhancement of heat exchanger, heat pipe and electronic components using graphene, Case Stud. Therm. Eng. 45 (2023) 102874.
[27] O'Dell, M., Mitchell, J., Beckman, W., 1984.Design method and performance of heat pumps with refrigerant-filled solar collectors.
[28] K. Pruess, Enhanced geothermal systems (egs) using co2 as working fluid—a novel approach for generating renewable energy with simultaneous sequestration of carbon, Geothermics 35 (2006) 351–367.
[29] Brown, D.W., 2000.A hot dry rock geothermal energy concept utilizing supercritical co2 instead of water, In: Proceedings of the Twenty-fifth Workshop on Geothermal Reservoir Engineering, Citeseer.233–238.
[30] P. Ahmed, A. Parahovnik, Y. Peles, Heat transfer of supercritical co2 near the critical condition inside a microchannel, in: Heat Transfer Summer Conference, American Society of Mechanical Engineers, 2023. V001T10A001.
[31] J. Wang, M. Evans, M. Belusko, C. Zhao, M. Liu, F. Bruno, Subcooling effect on the optimal performance for a transcritical co2 heat pump with cold thermal energy storage, Heat Mass Transf. 59 (2023) 1257–1275.
[32] M. Singh, S. Mahmoodpour, R. Ershadnia, M.R. Soltanian, I. Sass, Comparative study on heat extraction from soultz-sous-forêts geothermal field using supercritical carbon dioxide and water as the working fluid, Energy 266 (2023) 126388.
[33] J. Zhang, Y. Liu, H. Xu, J. Lv, Numerical investigation of heat transfer characteristics of supercritical co2 and water flow in 2d self-affine rough fractures, Appl. Therm. Eng. 241 (2024) 122342.
[34] Y. Li, G. Xin, B. Yuan, S. Zhang, W. Du, Experimental investigation on natural circulation heat transfer of supercritical co2 in a closed loop, Int. J. Heat Mass Transf. 200 (2023) 123503.
[35] M. Khoshvaght-Aliabadi, P. Ghodrati, O. Mahian, Y.T. Kang, Cfd study of rib-enhanced printed circuit heat exchangers for precoolers in solar power plants' supercritical co2 cycle, Energy 292 (2024) 130418.
[36] H. Dokmak, K. Faraj, J. Faraj, C. Castelain, M. Khaled, Geothermal systems classification, coupling, and hybridization: a recent comprehensive review, Energy Built Environ. (2024).
[37] R.B. Roka, A.J.P.D. Figueiredo, A.M.C.P. Vieira, J.C.D.P. Cardoso, A systematic review on shallow geothermal energy system: a light into six major barriers, Soils Rocks 46 (2023) e2023007622.
[38] H. Sadeghi, R.M. Singh, Driven precast concrete geothermal energy piles: current state of knowledge, Build. Environ. 228 (2023) 109790.

[39] J. Woods, A. Mahvi, A. Goyal, E. Kozubal, A. Odukomaiya, R. Jackson, Rate capability and ragone plots for phase change thermal energy storage, Nat. Energy 6 (2021) 295–302.
[40] E. Lemmon, M. Huber, M. McLinden, Nist Standard Reference Database 23: Reference Fluid Thermodynamic and Transport Properties-refprop, Version 8.0. National Institute of Standards and Technology, Standard Reference Data Program, Standard Reference Data Program, Gaithersburg, 2007.
[41] V.T. Nguyen, N. Wu, Y. Gan, J.M. Pereira, A.M. Tang, Long-term thermo-mechanical behaviour of energy piles in clay, Environ. Geotech. 7 (2019) 237–248.
[42] P.X. Jiang, Y.J. Xu, J. Lv, R.F. Shi, S. He, J. Jackson, Experimental investigation of convection heat transfer of co2 at super-critical pressures in vertical mini-tubes and in porous media, Appl. Therm. Eng. 24 (2004) 1255–1270.

Miss Linxiao Zhou earned her Bachelor of Engineering (Honours) in Civil Engineering from the University of Sydney in 2020. She joined Dr. Yixiang Gan's research group in same year and pursued a Master degree of Philosophy in Civil Engineering at the University of Sydney, graduating in 2022. Her research focuses on geothermal ground heat exchanger systems, emphasizing energy efficiency and sustainability through advanced Computational Fluid Dynamics (CFD) and Numerical Heat Transfer (NHT) techniques.